Available online at www.sciencedirect.com
ScienceDirect
Theoretical Population Biology 73 (2008) 319–331
Theoretical Population Biology
www.elsevier.com/locate/tpb

Effects of predation on host–pathogen dynamics in SIR models

Manojit Roy*, Robert D. Holt

Department of Zoology, University of Florida, 223 Bartram Hall, PO Box 118525, Gainesville, FL 32611-8525, USA

Received 6 December 2006
Available online 1 January 2008

Abstract

The integration of infectious disease epidemiology with community ecology is an active area of research. Recent studies using SI models without acquired immunity have demonstrated that predation can suppress infectious disease levels. The authors recently showed that incorporating immunity (SIR models) can produce a "hump"-shaped relationship between disease prevalence and predation pressure; thus, low to moderate levels of predation can boost prevalence in hosts with acquired immunity. Here we examine the robustness of this pattern to realistic extensions of a basic SIR model, including density-dependent host regulation, predator saturation, interference, frequency-dependent transmission, predator numerical responses, and explicit resource dynamics. A non-monotonic relationship between disease prevalence and predation pressure holds across all these scenarios. With saturation, there can also be complex responses of mean host abundance to increasing predation, as well as bifurcations leading to unstable cycles (epidemics) and pathogen extinction at larger predator numbers. Firm predictions about the relationship between prevalence and predation thus require one to consider the complex interplay of acquired immunity, host regulation, and foraging behavior of the predator.

Keywords: Host–pathogen; Predator–prey; Regulation; Immunity; Unstable cycles; Pathogen extinction

1. Introduction

Host–pathogen interactions do not occur in isolation. All host and pathogen species coexist with other species in communities, and community interactions can impart complex feedbacks on host–pathogen dynamics. There is an increasing realization of the need to examine the influence of interspecific interactions on infectious disease processes, in order to develop a better understanding of pathogen persistence and dynamics, and the role of pathogens in communities (Collinge and Ray, 2006; Holt and Dobson, 2006). For example, species composition and diversity can affect host and pathogen coexistence and disease risk (de Castro and Bolker, 2005; Keesing et al., 2006). Pathogens often infect multiple host species (Woolhouse et al., 2001; Dobson, 2004), and hosts can be infected by multiple pathogen species (Holt and Dobson, 2006; Rohani et al., in press). Furthermore, infectious disease dynamics can be influenced by the entire web of trophic interactions in the community.

A particularly important class of trophic interactions is predation. Generalist predators can alter disease incidence by attacking infected prey (Hudson et al., 1992; Arneberg et al., 1998; Dwyer et al., 2004; Ostfeld and Holt, 2004; Hall et al., 2005). Packer et al. (2003), Ostfeld and Holt (2004), and Hall et al. (2005) used simple models to suggest that reduction in predator numbers can increase disease incidence, and that a potentially harmful consequence of predator removal could be enhanced "spillover" infection to novel host species, including humans (also see Holt and Dobson, 2006). Hall et al. (2005) demonstrated that selective attacks on infected hosts can inhibit pathogen persistence, and that unstable dynamics could emerge with saturating functional responses. All these studies to date have considered relatively simple SI ("Susceptible–Infective") models without acquired immunity, in which the host population is assumed to consist of only two disease classes: susceptible and infective individuals. In SI models, predation on hosts usually lowers disease prevalence for two distinct reasons. First, predation on infected individuals reduces their expected lifespan, thereby lowering the number of secondary infections spawned by each primary infection. Second, predation on susceptible hosts reduces host

* Corresponding author.
E-mail addresses: roym@ufl.edu (M. Roy), rdholt@zoo.ufl.edu (R.D. Holt).

0040-5809/$ - see front matter © 2008 Elsevier Inc. All rights reserved.
doi:10.1016/j.tpb.2007.12.008

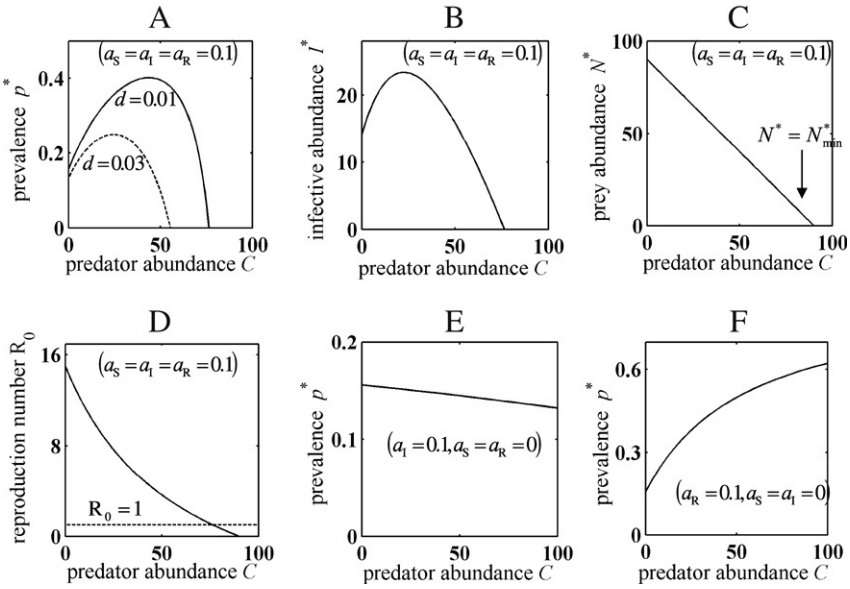

Fig. 1. Impacts of predation upon measures of disease load and dynamics, for model (1). A, B, C and D show, respectively, the equilibrium pathogen prevalence p^* (from (4e)), equilibrium abundance of infective class I^* (from (4b)), total prey/host abundance N^* (from (4d)) and basic reproduction number R_0 (from Eq. (5)), plotted against predator abundance C. The mortality rates are given by (3) and indiscriminate predation ($a_S = a_I = a_R = 0.1$) is assumed. The density dependence parameter $d = 0.01$. E and F show plots of prevalence p^* versus C under, respectively, selective predation on the infective prey alone ($a_I = 0.1, a_S = a_R = 0$) and the recovered prey alone ($a_R = 0.1, a_S = a_I = 0$). The dashed plot in A again assumes indiscriminate predation, but uses a different value for density dependence ($d = 0.03$). The dashed line in D denotes the threshold $R_0 = 1$ for pathogen persistence. Other parameter values are $b = 10$, $m_0 = 1$, $\beta = 1$ and $\gamma = 5$.

productivity, which in turn lowers the equilibrial density of infections sustained in the population.

In a recent paper, Holt and Roy (2007) have shown that in SIR ("Susceptible–Infective–Recovered") models with an immune host class, predators can at times lead to an *increase* in equilibrial pathogen prevalence. They demonstrated that the overall pattern relating prevalence to predator abundance (assumed here to scale the consumption of host by the predator, that is, predation pressure) can be "hump-shaped". If initial predator numbers are low, increasing predation can boost disease prevalence, but beyond a certain abundance of predators, further increases in predation reduce prevalence (see, for example, Fig. 1A). This effect arises due to the combined interplay of predation, negative density dependence, and the presence of an immune class. When host abundance is strongly regulated by density dependence, predation on immune individuals can boost the rate of recruitment of susceptible hosts (for instance, reduced intraspecific resource competition increases fecundity), which in turn can generate higher rates of infection, at least at low levels of predation.

The present paper has a two-fold objective. First, we explore in more detail the generality of the non-monotonic pattern of prevalence reported in Holt and Roy (2007), by considering a wide range of realistic extensions of the basic SIR model. We explore in detail host–pathogen dynamics with logistic density-dependent regulation in host birth rates, and two alternative disease transmission mechanisms — density-dependent transmission, and frequency-dependent transmission. The papers cited above (e.g. Holt and Roy, 2007) assume that predator numbers are independent of the focal prey species. We relax this assumption and consider a predator that is a specialist on the host. We also consider a broader range of predator foraging behaviors, including saturating (Holling type II) responses. Finally, we replace logistic host regulation with dependence on an explicit resource, providing an indirect form of regulation. We demonstrate that the hump-shaped pattern of prevalence remains qualitatively robust across all these modifications of the basic disease model.

As the second objective of this paper, we analyze the effect of predation on the dynamics of host–pathogen interaction in SIR models, assuming a saturating response to predation. We show that the interplay of predation pressure, host density dependence and saturating functional response generates a variety of effects, including alternative stable states, transitions from stable equilibria to unstable cycles, and pathogen extinction via homoclinic bifurcation. These results complement the earlier study of an SI model by Hall et al. (2005). Our results suggest that unstable dynamics may be a generic feature of systems that incorporate a mixture of predation and parasitism, and that changes in predation can influence the likelihood of epidemic outbreaks as well as average disease prevalence.

2. The model

We begin by assuming (as did earlier studies, Packer et al., 2003; Ostfeld and Holt, 2004; Hall et al., 2005; Holt and Roy, 2007) that the predator is a generalist whose dynamics are governed by factors other than the focal prey. Predator abundance, C, then enters the model equations as a free parameter. Later we relax this assumption and consider a predator that is a complete specialist with a Lotka–Volterra type interaction with a prey species that also supports a specialist pathogen.

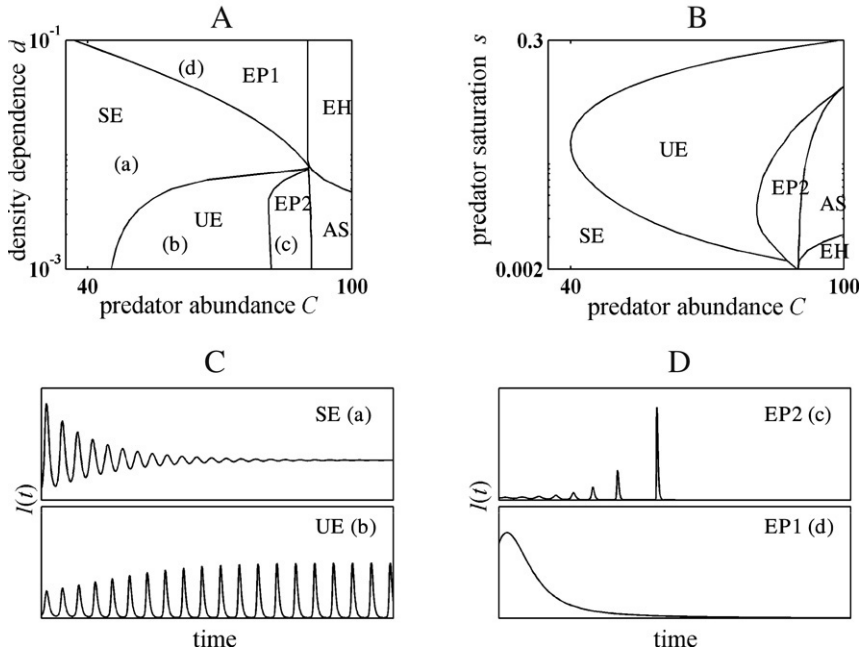

Fig. 2. Host–pathogen dynamics with predator saturation. A and B, Bifurcation diagrams as, respectively, the host density dependence and predator saturation are varied with predator abundance C. The saturation value in A is chosen to be $s = 0.01$, and the density dependence in B is chosen to be $d = 0.002$. The dynamical regimes in the parameter space are shown as non-overlapping domains labeled SE (stable equilibrium), UE (unstable equilibrium with persistent cycles), EP1 (pathogen extinction via a stable transition), EP2 (pathogen extinction via homoclinic bifurcation), AS (alternative stable states) and EH (host extinction). C and D, Illustrative examples of time series for infective abundance $I(t)$, for values of d and C indicated by the locations (a), (b), (c) and (d) in Fig. 2A. The data are obtained by numerically integrating Eq. (1) with the assumption of saturating mortality rates (given by Eq. (7), with $s = 0.01$) and indiscriminate predation ($a_S = a_I = a_R = 0.1$). Other model parameters used are $b_S = 10$, $b_I = 0.1$, $b_R = 1$, $m_0 = 1$ and $\beta = \gamma = 1$.

An SIR model with logistic host regulation experienced in fecundity is as follows:

$$\begin{aligned}\frac{dS}{dt} &= (b_S S + b_I I + b_R R)(1 - dN) \\ &\quad - m_S(S, I, R, C)S - \beta SI, \\ \frac{dI}{dt} &= \beta SI - [\gamma + m_I(S, I, R, C)]\, I, \\ \frac{dR}{dt} &= \gamma I - m_R(S, I, R, C)R.\end{aligned} \tag{1}$$

Here S, I and R respectively denote the numbers of susceptible, infective and recovered (and immune) individuals in the prey/host population (total abundance $N = S + I + R$); b_S, b_I, b_R are maximum birth rates in the absence of density dependence, and m_S, m_I, m_R the per capita death rates, of the three respective classes of hosts; β is the disease transmission coefficient; γ is the rate of recovery from infection; and finally, d is the strength of logistic density dependence in prey births (to preclude negative births, we impose $N < 1/d$ throughout).

In general, prey death rates are composed of intrinsic and predation-induced mortality, and depend on both prey and predator abundances. These death rates can be represented formally as follows:

$$m_{S,I,R}(S, I, R, C) = m_{S0,I0,R0} + f_{S,I,R}(S, I, R, C). \tag{2}$$

In this notation m_{S0}, m_{I0}, m_{R0} denote the density-independent, and f_S, f_I, f_R the density-dependent, components of prey mortality. We make the reasonable assumption that mortality rates increase with predation pressure, so $\partial f/\partial C > 0$. For example, the standard per capita mass-action (Holling type I) interaction between the predator and the prey assumes that f is a linear function of C, and independent of prey density. Expression (2) then becomes

$$m_{S,I,R}(S, I, R, C) = m_{S0,I0,R0} + a_{S,I,R}C, \tag{3}$$

where a_S, a_I and a_R are predator attack rates on the three prey classes.

Unless stated otherwise (for instance in Figs. 2 and 3), for simplicity we assume equal birth and death rates of the prey classes: $b_S = b_I = b_R \equiv b$ and $m_S = m_I = m_R \equiv m$. In effect, this assumes that the pathogen is a commensal, with no demographic impact on its host. (Numerical studies suggest that relaxing this assumption does not affect our qualitative conclusions, see Fig. 3.) If the density-independent mortality m_0 is same for all prey classes, then from (3) $m_S = m_I = m_R$ implies $a_S = a_I = a_R = a$; that is, the predator attacks susceptible, infective and recovered prey indiscriminately. Assuming m to be independent of prey abundance (as in (3)), Eq. (1) can be solved for the endemic equilibrium (S^*, I^*, R^*) as follows:

$$S^* = \frac{1}{\beta}(\gamma + m), \tag{4a}$$

$$I^* = \frac{m}{\beta}(\mathrm{R}_0 - 1), \tag{4b}$$

$$R^* = \frac{\gamma}{m} I^*, \tag{4c}$$

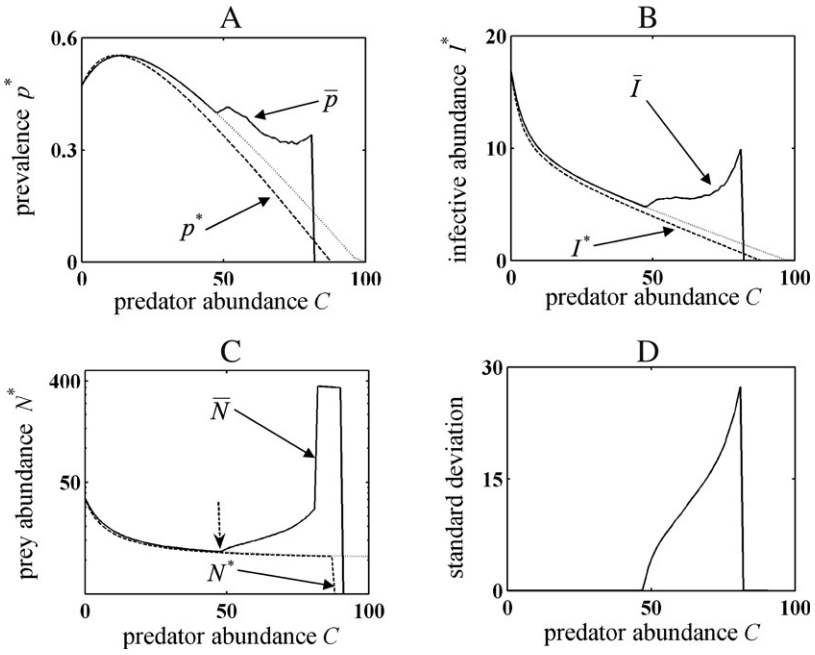

Fig. 3. Impacts of predation upon measures of disease load in unstable hosts, with saturating response and indiscriminate predation ($a_S = a_I = a_R = 0.1$). A, B and C show, respectively, the time-averaged values of pathogen prevalence $\bar{p}$, infective abundance $\bar{I}$ and total prey abundance $\bar{N}$. D shows the standard deviation of the time series $N(t)$ against predator abundance C. Each data point is computed by averaging the corresponding time series over 500 time units in the stationary regime (ignoring transients). The broken vertical arrow at $C \cong 48$ in Fig. 3C denotes the Hopf bifurcation point at which the stable equilibrium changes to unstable cycles. The corresponding equilibrial plots with (dotted line) and without saturation (dashed line, denoted by p^*, I^* and N^*) are overlaid in A–C. The saturation and density dependence parameters used are $s = 0.01$ and $d = 0.002$. Other model parameters are the same as in Fig. 2.

$$N^* = S^* + I^* + R^* = \frac{1}{d}\left(1 - \frac{m}{b}\right), \tag{4d}$$

$$p^* = \frac{I^*}{N^*} = \frac{m}{(\gamma + m)}\left(1 - \frac{1}{\mathrm{R}_0}\right). \tag{4e}$$

In these expressions, R_0 denotes the basic reproduction number for the pathogen:

$$R_0 = \frac{\beta S^*_{\mathrm{DFE}}}{\gamma + m} = \frac{\beta}{d(\gamma + m)}\left(1 - \frac{m}{b}\right), \tag{5}$$

where $S^*_{\mathrm{DFE}} = (1/d)(1 - m/b) = N^*$ gives the disease-free equilibrium expression for wholly susceptible host abundance. From (4d), the prey can persist under predation only if $b > m$. The feasibility condition for the equilibrium (4) is the well-known threshold condition $R_0 > 1$, which from (5) is stronger than the condition $b > m$ for host survival. Equilibrium (4) is locally stable (see Appendix A for an analytical derivation of the stability conditions).

The minimum equilibrial prey abundance N^*_{min} needed for pathogen invasion is obtained from the condition $R_0 > 1$:

$$N^* > N^*_{\mathrm{min}} \equiv \frac{1}{\beta}[\gamma + m(C)]. \tag{6}$$

If mortality is sufficiently high, the pathogen may be excluded. Thus, predation can indirectly benefit the prey by depressing its abundance, thereby potentially keeping the pathogen at bay.

3. Results

Fig. 1A–D show illustrative plots of equilibrial abundances, and the basic reproduction number R_0, against predator abundance C. These plots assume that prey mortality is given by expression (3), and that the predator attacks the prey indiscriminately ($a_S = a_I = a_R$). Both the equilibrium prevalence p^* (Fig. 1A) and the infective abundance I^* (Fig. 1B) "exhibit a unimodal hump shape", increasing for low predation pressure, and then decreasing for sufficiently high values of C. Note that R_0 monotonically decreases with increasing C (see Fig. 1D), as expected from (5), and more rapidly so when p^* and I^* increase. Thus, R_0 and disease levels can respond in opposite directions to changes in predation.

The pathogen becomes extinct (I^*, $p^* = 0$) when predator abundance exceeds a threshold value C_{th}, found by setting $\mathrm{R}_0 = 1$ in (5) and substituting $m = m_0 + aC$:

$$C_{\mathrm{th}} \equiv \frac{1}{a(\beta + bd)}[b(\beta - \gamma d) - m_0(\beta + bd)].$$

Increasing density dependence (d) lowers C_{th} (the dashed line in Fig. 1A). The threshold predator abundance C_{th} is where the total prey abundance N^* drops to the minimum value N^*_{min} (from (6)) that can support the pathogen (the downward arrow in Fig. 1C). Further increases in C eventually drive the prey to extinction (see Fig. 1C).

Numerical studies suggest that the unimodal pattern for the prevalence in Fig. 1A does not require the strict assumption of equal attack rates on all prey classes, or the assumption of equal mortality or birth rates across classes. The only requirement appears to be that the predator must attack the recovered prey ($a_R > 0$), along with either the susceptible or the infective prey ($a_S > 0$ or $a_I > 0$), or both. Closed-form analytical expressions of the equilibrium for such non-

symmetric cases are very cumbersome, but the overall reason for the hump-shaped relation of prevalence to predation can be intuitively argued as follows. If the predator completely ignores the recovered prey, then whether it attacks the susceptible or the infective prey (or both), I^* and p^* should always decrease monotonically with increasing C (for the same reasons as in the SI model discussed by Packer et al., 2003). Fig. 1E shows a typical plot of p^* when the predator selectively attacks only the infective prey. By contrast, if the predator ignores both susceptible and infective prey, and attacks only the recovered prey, the effect of predation on the pathogen is indirect, via relaxation of density-dependent constraints on recruitment. Numerical studies suggest that in this case, the equilibrium prevalence p^* increases with C relatively fast at low level of predation; however, the effect eventually saturates, because the recovered class is depleted at sufficiently high predation. Fig. 1F shows a typical plot of p^* within the range $0 \leq C \leq 100$. If the predator attacks the recovered prey along with either susceptible or infective prey, one observes a hump-shaped pattern, in effect blending the patterns shown in Figs. 1E and F.

3.1. Predator saturation and prey cycles

The above results assume that the average predation risk of a prey individual does not depend on prey abundance (prey mortality was given by (3)). While this may be true at low prey density, at high prey density the attacks inflicted by an individual predator should usually saturate. A standard way to model saturating predator responses is the generalized Holling disk equation (e.g., Turchin, 2003, p. 82), which in our case is given by $f_{S,I,R}(S, I, R, C) = a_{S,I,R}C/(1 + a_S h_S S + a_I h_I I + a_R h_R R)$ in expression (2), where h_S, h_I and h_R are the handling times for the three prey classes. For simplicity we assume the "half-saturation constant" $(ah)^{-1}$ to be equal for all prey classes, so $a_S h_S = a_I h_I = a_R h_R \equiv s$. Expression (2) then becomes

$$m_{S,I,R}(N, C) = m_{S0,I0,R0} + \frac{a_{S,I,R}C}{1 + sN}, \tag{7}$$

where s is the saturation parameter.

Because of the non-linear functional response, interesting dynamics such as alternative stable states and unstable cycles may now occur. Hall et al. (2005) showed these effects for an SI model with a saturating generalist predator. Because our SIR model includes this SI model as a limiting case (viz., when $\gamma \to 0$), it is clear that it too should exhibit similar dynamics. In absence of the pathogen, at low predator numbers C the prey exists at a stable equilibrial density, whereas at sufficiently high predation only host extinction results. In between, alternative stable states comprising these two stable branches can occur, bracketed by a transcritical bifurcation on the left and a fold bifurcation on the right (as in Fig. 1A of Hall et al., 2005). Addition of the pathogen gives rise to a rich array of additional behaviors, including host–pathogen coexistence via unstable cycles, as well as instabilities leading to pathogen extinction.

Persistence and stability are determined by the joint interplay of negative density dependence (d), the strength of the saturating response (s) and predator abundance (C). Fig. 2A–B illustrate the bifurcation characteristics of the SIR model with indiscriminate predation, as a function of d, s and C. In these results we do not assume the pathogen to be a mere commensal (indeed, as pointed out later in the Discussion, instability cannot arise in our model in this case). Instead, now the fecundity of the different host classes have the relationship $b_I < b_R < b_S$, with infected individuals being most affected by the disease, but also with a legacy impact of past infection on the fecundity of recovered individuals. In Fig. 2A we keep s fixed ($s = 0.01$) while using d and C as bifurcation parameters, and in 2B the parameters s and C are varied with a fixed d ($d = 0.002$). We used the software package "MatCont" (Dhooge et al., 2003) to trace these bifurcations. The different dynamical regimes in both these plots are labeled as follows: "SE" refers to a stable equilibrium, "UE" to an unstable equilibrium leading to sustained cycles, "EP1" to pathogen extinction via stable transition, "EP2" to pathogen extinction via a homoclinic bifurcation, "AS" to alternative stable states (with the host dynamics either reaching a stable positive equilibrium or extinction, depending on the initial density), and finally, "EH" to the extinction of host via a stable bifurcation. High density dependence tends to stabilize the dynamics, as expected; conversely, cycles appear for low values of d (SE and UE, respectively, in Fig. 2A). As predation is increased at these low levels of density dependence, the unstable cycles grow in amplitude until the pathogen is driven to extinction via a homoclinic bifurcation, and the disease-free host returns to its stable equilibrium (EP2); further increases in C cause the host to enter the domain of alternative stable states (AS) via a transcritical bifurcation, where it approaches either an equilibrial abundance or extinction depending on its initial density. By contrast, increasing predation pressure at high values of d gives rise to stable transitions from equilibrial host–pathogen coexistence (SE) to, first, pathogen extinction (EP1), and then at sufficiently high predation, host extinction (EH). Fig. 2C–D show times series examples for infective hosts, $I(t)$, to illustrate some of these dynamical regimes; the locations of the d and C values used in these examples are correspondingly labeled by (a), (b), (c) and (d) in Fig. 2A. In Fig. 2C, the pathogen persists, whereas in Fig. 2D, the pathogen goes extinct, either because of increasing instability due to a homoclinic orbit (the upper panel), or because there is a smooth approach to extinction (the lower panel).

The interplay of saturation s and predator abundance C leads to a similar set of dynamical outcomes as shown by the bifurcation diagram in Fig. 2B (except EP1 does not occur, within the range of parameter values considered here). For very low s, the saturating response is not strong enough to destabilize the dynamics. At high values of s, the predator has a correspondingly weak effect, and so loses control of the host–pathogen dynamics, which then returns to its inherent stability. The dynamics are thus unstable for intermediate values of s (UE in Fig. 2B) at moderate levels of predation, but the dynamics change to homoclinic pathogen extinction (EP2) and then alternative stable states (AS) (with the host alone being present), as predation pressure increases.

The origin of these cycles can be understood in terms of the interplay of regulation of the host population by both pathogen and predation. The two processes of prey escape and overexploitation that create cycles in standard predator–prey models under saturating predation (Murdoch et al., 2003, p. 39–40) are also present in our host–pathogen model. As the number of susceptible hosts increases above its equilibrium, there is a corresponding decline in mortality (due to the saturating functional response); the lag in the response of the pathogen (in converting susceptible individuals to infective individuals) then permits the susceptible sub-population to rise even further. Eventually the infection catches up, and the susceptible prey is then depleted through a rapid rise in infection. As the susceptible abundance is pushed below its equilibrium, there is increased per capita mortality from predation, and also the high infective abundance keeps draining them away (analogous to overexploitation), until the pathogen begins to "starve" because of a shortage of susceptible hosts, and the infective numbers then start to drop. Note that we have assumed indiscriminate predation on all prey classes; a decrease in the susceptibles thus also indirectly increases mortality on the infectives (because predators are less saturated). Hall et al. (2005) previously showed that unstable dynamics in an SI model occurred, assuming selective predation upon infected individuals. Our results show that the assumption of selective predation is not required for instability in an SIR model. All three host classes in effect are indirect mutualists, mediated through the predator's saturating functional response; an increase in any one of them decreases mortality in the others. This (+, +) interaction contributes to the observed instability.

Within the unstable regime, in extensive numeric studies we did not find any evidence of aperiodic or irregular cycles, such as chaotic fluctuations; the value of the leading Lyapunov exponent obtained by linearizing Eq. (1) with the mortality rates given by Eq. (7) appears to be negative within the entire parameter space in the unstable regime (see Appendix B). This of course does not guarantee that such behaviors may not be present in a small region of parameter space.

Given instability, numerical integration permits us to assess how the time-averaged quantities $\bar{I}$, $\bar{N}$ and $\bar{p} = \bar{I}/\bar{N}$ depend on the level of predation. Because of non-linearity, time-averaged abundances in unstable ecological models can behave quite differently than do equilibria in response to changes in parameter values (Abrams, 2002). The solid line plots in Fig. 3A–C illustrate an example for indiscriminate predation ($a_S = a_I = a_R$) for $s = 0.01$. These figures also include corresponding equilibrial plots with the same value for saturation (dotted lines) and with s set equal to zero (dashed lines). These plots assume unequal prey birth rates as in Fig. 2, so that $b_I < b_R < b_S$. (The expressions for p^*, I^* and N^* in the absence of saturation with these unequal birth rates are accordingly a good deal more complex than (4a)–(4e), and including them is not useful here; we used Mathematica to obtain equilibrial plots with and without saturation in Fig. 3A–C).

With uniform prey births, I^* and p^* both show qualitatively similar unimodal patterns in relation to predator abundance (Fig. 1A–B). With unequal birth rates for different prey classes, however, this similarity no longer holds. Fig. 3A–B provide an example showing that infective abundance and prevalence can move in opposite directions, at least over some range of predation pressure, when different host classes have different fecundities: for low values of C, $\bar{p}$ and p^* increase even as $\bar{I}$ and I^* decline rapidly. Such contrasting patterns in I^* and p^* in response to changes in predation can also occur even in the absence of density dependence (see Fig. A1, A and B in Holt and Roy, 2007). Thus, the overall disease burden (as measured by infective abundance) in the prey population may decrease, even as the *proportion* of the infected population (prevalence) increases, with increasing predation. The reason is that within this range of increasing C, total prey abundance decreases *at a faster rate* than does the infective abundance.

Time-averaged prevalence $\bar{p}$ with predator saturation again exhibits a hump shape similar to the no-saturation plot for p^*, but the similarity ends at $C = 48$; the pattern becomes more complex thereafter (Fig. 3A, solid line). This is also the point beyond which, for the case with saturation, the dynamics become unstable, and there is a divergence between the patterns of equilibrial abundance and time-averaged abundance (solid and dotted lines in Fig. 3A–C). Both $\bar{I}$ and $\bar{N}$ continue to decrease until $C = 48$; afterwards, they begin to *increase* with C (Fig. 3B and C, solid line). The value $C = 48$ in this example (indicated by a broken vertical arrow in Fig. 3C) denotes the Hopf bifurcation point for Eq. (1) in the presence of predator saturation, across which the stable host–pathogen equilibrium becomes unstable, and sustained cycles begin to appear in the dynamics (see Fig. 2A). Beyond this point, the magnitude of the instability rapidly magnifies with increasing predation pressure, as shown in Fig. 3D, which plots the standard deviation of the time series $N(t)$ against C. An increase in mean prey population size with increasing per capita mortality in the unstable regime regularly occurs in unstable ODE models of predator–prey dynamics (Rosenzweig, 1971; Abrams, 2002). Multimodal relationships between mean abundance and a parameter value in the unstable regime, for example at $C \geqslant 48$ in Fig. 3A (the solid line plot), have also been observed in other consumer–resource models (e.g. Abrams, 2002). The pathogen becomes extinct via homoclinic bifurcation (see Fig. 2A) when the predator abundance C crosses a threshold (in this example $C = 82$), and the prey then stabilizes at high abundance (Fig. 3C, solid line; note the logarithmic vertical scale). As C is increased further, the prey, too, becomes extinct (in this example, at $C = 91$). Thus, responses of prey abundance to changes in predator abundance can be large and non-monotonic, when an infectious disease is present, and mean prevalence can show complex responses to changes in predation when the dynamics are unstable.

4. Alternative model scenarios

4.1. Predator interference

One weakness of the above model is that we assumed the predator attack rates to be independent of predator density.

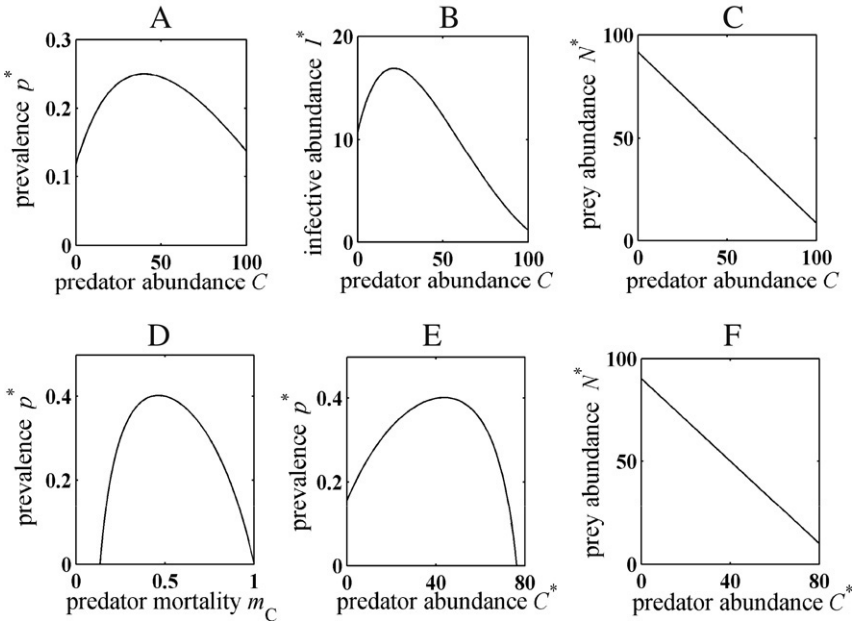

Fig. 4. Effects of predation upon disease loads with alternate scenarios. A, B and C show, respectively, the plots of equilibrium prevalence p^*, infective abundance I^* and total prey abundance N^* against predator numbers C under frequency-dependent disease transmission, assuming indiscriminate predation. Model parameters are $b = 12$, $m_0 = 1$, $\beta = 20$, $\gamma = 5$, $a = 0.1$, and $d = 0.01$. D, E and F show similar results for host–pathogen dynamics with a specialist predator. D, Equilibrium prevalence p^* is plotted against predator mortality rate m_C (using expression (11c)). E and F, Prevalence p^* and total prey abundance N^* are now plotted against the equilibrium predator abundance C^* (using (11a)–(11c)). Model parameters are $b = 10$, $\beta = 1$, $\varepsilon = 0.1$; others are same as in Fig. 4A–C.

More generally, predators can directly interfere with each other. We explored the following modification of (7) to include predator interference

$$m_{S,I,R}(N, C) = m_{S0,I0,R0} + \frac{a_{S,I,R}C}{1 + sN + iC},$$

where $i = aq$ is the interference parameter, with q denoting a wasting time due to predator interference (DeAngelis et al., 1975; Turchin, 2003, p. 85–86). Introducing such a functional response has a modest quantitative effect of reducing the impact of predation on mean disease levels in the prey (interference provides another source of direct density dependence), without any qualitative change in the relationship of predation to disease prevalence (details not shown).

4.2. Frequency-dependent pathogen transmission

The density-dependent disease transmission term βSI assumes that every individual directly interacts with every other individual in the host population, so that the contact rate increases with population size. This may be a reasonable approximation for small populations, but does not work well in large and viscous populations where an individual may directly interact only with a small fraction of the population. In this case, the contact rate saturates with increasing population size. The frequency-dependent transmission term $\beta SI/N$ in place of βSI in Eq. (1) captures this feature of transmission dynamics (to save space, these otherwise identical equations are not repeated here).

As before, for simplicity we again assume that the pathogen is in effect a commensal: $b_S = b_I = b_R \equiv b$ and $m_S = m_I = m_R \equiv m$, and also assume that the prey mortality m is independent of prey abundance. The (locally) stable endemic equilibrium now becomes:

$$N^* = \frac{1}{d}\left(1 - \frac{m}{b}\right), \qquad I^* = \frac{m(b-m)(\mathrm{R}_0 - 1)}{bd\beta},$$
$$p^* = \frac{I^*}{N^*} = \frac{m}{\beta}(\mathrm{R}_0 - 1). \tag{8}$$

The expression for N^* is the same as (4d) under density-dependent transmission. The basic reproduction number R_0 in (8) is given by

$$R_0 = \frac{\beta}{\gamma + m}, \tag{9}$$

which does not depend on host abundance (in contrast with expression (5) for density-dependent transmission), and hence the pathogen can deterministically persist in very small host populations (there is no cut-off host population size $N^*_{\min}$ unlike (6)). However, if mortality increases with predator abundance, there will be a threshold predator abundance, above which the pathogen disappears. The equilibrium (8) is feasible if $b > m$ and $\mathrm{R}_0 > 1$. Note that even though the expressions for p^* in (8) and I^* in (4b) are identical, it is easy to see from the definition of R_0 in (9) that p^* is always bounded below 1, as long as $\mathrm{R}_0 > 1$.

The equilibrial infective abundance I^* and prevalence p^* both exhibit a qualitatively similar hump shape as observed above (this was noted briefly in Holt and Roy, 2007), as illustrated in Figs. 4A and B. Allowing infected individuals to have lower birth rates and higher mortality does not alter this basic pattern (details not shown). Fig. 4C shows a plot of N^*

versus C that is similar to Fig. 1C (except that Fig. 4C assumes a slightly larger b).

If we now permit the predator's attack rate to be described by a saturating functional response, we again find a range of dynamical behaviors comparable to those discussed above for density-dependent transmission (details not shown).

4.3. Predator numerical response (specialist predator)

Until now we have assumed that the predator is a generalist, whose numerical dynamics are decoupled from the focal prey. This assumption has allowed us to simplify the equations by treating the predator population size C as simply a parameter. Such generalist predators are found in many communities; for example, cats prey on rats but also subsist on a variety of other resources, and birds of prey such as hawks and eagles feed on prey species across a wide range of taxa. However, many predators exhibit some preference for a particular prey, and respond dynamically to changes in the abundance of that prey (e.g., the Canadian lynx on the snowshoe hare). A canonical model of a specialist predator–prey interaction, where the predator completely depends on a single prey species, is the Lotka–Volterra model. Several authors have recently studied models that combine specialist predator–prey dynamics with disease in the prey, but none has considered the impact of acquired immunity (Chattopadhyay and Arino, 1999; Xiao and Chen, 2001; Chattopadhyay et al., 2003; Hethcote et al., 2004; Braza, 2005; Hall et al., 2005). Most of these authors, moreover, have assumed selective predation on the infective class alone. The main focus of these papers was to determine conditions for stable coexistence equilibria for the pathogen and predator; some have also studied the instability of the equilibrium via Hopf bifurcation, assuming a saturating functional response. (Han et al. (2001) did examine an SIR disease model with predators, but they allowed both prey and predator to be infected by the pathogen; this is very different from the scenarios we are considering here, where the predators are solely mortality sources for the prey.) It is thus useful to examine the consequences of changing our assumption about predator regulation on the disease prevalence in a host/prey species.

Rewriting Eq. (1) with an additional equation for the predator abundance, and using expression (3) for prey mortality, gives

$$\begin{aligned}
\frac{dS}{dt} &= bN(1-dN) - (m_0 + aC)S - \beta SI,\\
\frac{dI}{dt} &= \beta SI - (\gamma + m_0 + aC)I,\\
\frac{dR}{dt} &= \gamma I - (m_0 + aC)R,\\
\frac{dC}{dt} &= \varepsilon aNC - m_C C.
\end{aligned} \tag{10}$$

Here, for simplicity we have as before assumed that $b_S = b_I = b_R \equiv b$, $m_S = m_I = m_R \equiv m$, that the predator feeds indiscriminately on all prey types, and that the predator conversion efficiency ε is same for all prey types; m_C denotes the per capita predator mortality rate. We can solve Eq. (10) for the stable endemic equilibrium, leading to

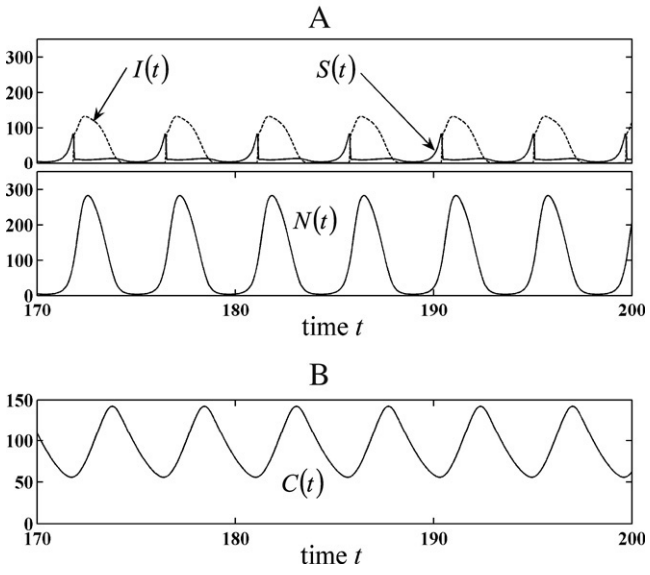

Fig. 5. Illustrative example of time series for both prey abundance $N(t)$ and predator abundance $C(t)$ in the model (10) with a specialist predator and a saturating response. The plot also shows the time series of susceptible (solid line) and infected prey numbers (broken line). We assume indiscriminate predation ($a_S = a_I = a_R = 0.1$) as before, and other model parameters are $d = 0.002$, $s = 0.005$, $m_C = 0.5$; the other parameters are the same as in Fig. 4D–F.

$$N^* = \frac{m_C}{a\varepsilon}, \qquad I^* = \frac{b}{\beta}(1 - dN^*)(\mathrm{R}_0 - 1), \tag{11a}$$

$$C^* = \frac{1}{a}[b(1 - dN^*) - m_0], \tag{11b}$$

$$p^* = \frac{I^*}{N^*} = \frac{b}{\beta}\frac{(1 - dN^*)}{N^*}(\mathrm{R}_0 - 1), \tag{11c}$$

where R_0 is given as

$$\mathrm{R}_0 = \frac{\beta N^*}{\gamma + m_0 + aC^*} = \frac{\beta N^*}{\gamma + b(1 - dN^*)}.$$

The above equilibrium is feasible if $N^* < 1/d$, $b > m_0$ and $\mathrm{R}_0 > 1$.

Prey abundance N^* increases linearly, whereas predator abundance C^* decreases linearly, with increasing predator mortality rate m_C. Fig. 4D shows equilibrium prevalence p^* against predator mortality m_C, and Fig. 4E plots p^* against the equilibrium predator abundance C^* (which varies with m_C via (11a) and (11b)). Prevalence p^* exhibits the now familiar hump shape in both plots. Fig. 4F shows a linear decay of N^* versus C^*, as expected from (11b).

Non-linear functional responses lead to algebraically intractable equations for the equilibrium. Using the saturating mortality function (7) in Eq. (10), the system shows a broadly similar dynamic instability as in Fig. 2, with the difference that now the predator also cycles in concert with the prey. Fig. 5 shows an example where both the prey and predator cycle. The instability becomes pronounced both with low density dependence d and intermediate values of saturation

s, comparable to the patterns in Fig. 2A–B. For instance, as predation pressure increases at low density dependence, the pathogen is driven extinct via large-magnitude cycles. On the other hand, at higher density-dependent regulation, increasing predation pressure again drives the pathogen to extinction, but via stable transitions (details will be presented elsewhere). It is well known that a specialist predator with numerical responses to its prey combined with a saturating functional response, feeding upon a prey with weak direct density dependence, can generate limit cycles in both predator and prey numbers (Rosenzweig, 1971). Our results with generalist predators, and those of Hall et al. (2005), show that cycles in prey numbers and disease loads can emerge even if the predator has fixed abundance, but has a saturating functional response. The Lotka–Volterra predator–pathogen–prey model with a saturating functional response thus combines two distinct mechanisms which can contribute to unstable dynamics.

It should be noted that in this system, there is a problem in species coexistence. The predator and pathogen both feed on healthy hosts, and in addition the predator attacks infected prey. The interaction among host, pathogen and predator thus is an example of intraguild predation (Holt and Polis, 1997). The condition for the coexistence of pathogen and predator is (see Appendix C)

$$\frac{b+\gamma}{bd+\beta} < N^* < \frac{1}{d}\left(1-\frac{m_0}{b}\right). \tag{12}$$

Thus, the condition for pathogen and predator coexistence sets a bound for the equilibrial prey/host abundance, when the predator is present. The expression on the right is prey abundance when the predator is absent. The inequality on the left emerges from the conditions for invasion by the pathogen into an equilibrium with both the predator and host being present.

Considering the conditions for mutual invasion, the pathogen is vulnerable to exclusion if the predator has a high attack rate, or low mortality rate, or is efficient in converting captured prey biomass into predator births. At sufficiently high birth rates (e.g., in a highly productive environment) the condition for pathogen persistence reduces to $d > a\varepsilon/m_C$, which is independent of the rate of disease transmission (β). The reason is that density dependence reduces the number of predators that can be sustained by the prey, thus moderating the mortality experienced by infected hosts. When the prey is potentially highly productive, this indirect constraint on predator numbers and hence on the mortality inflicted on infected individuals is crucial for pathogen persistence. (Note that these relatively simple expressions assume that the pathogen has a negligible impact on the demography of its host. Permitting host impacts of infection leads to much more cumbersome algebraic expressions.)

Lotka–Volterra models of intraguild predation can exhibit unstable dynamics, even with linear functional responses (Holt and Polis, 1997). We have not found an example of this phenomenon for the symmetrical case leading to the equilibrium described by (11). The issue of unstable dynamics and alternative equilibria in asymmetrical cases where the pathogen does impact its host, or with saturating functional responses, deserves further attention.

Other authors have previously explored systems where specialist natural enemies (e.g. parasitoids) and specialist pathogens interact (e.g., Anderson and May, 1986; Hochberg et al., 1990). Borer et al. (2007) point out that this suite of interactions parallels in many ways, intraguild predation. However, this issue to our knowledge has not been examined for systems in which hosts have acquired immunity.

4.4. An explicit resource for the prey

We have assumed that the prey is regulated by direct density dependence on its fecundity. We now consider the case where the prey consumes an explicit resource and density dependence emerges indirectly from the resource–consumer interaction. (This is a "semi-chemostat" model, which differs from the standard chemostat model in that the consumer does not have the same wash-out rate as the resource; see Murdoch et al., 2003, p. 213.) The equations are as follows:

$$\begin{aligned}
\frac{dF}{dt} &= \Lambda - (w+cN)F,\\
\frac{dS}{dt} &= bNF - m(C)S - \beta SI,\\
\frac{dI}{dt} &= \beta SI - [\gamma + m(C)]I,\\
\frac{dR}{dt} &= \gamma I - m(C)R,
\end{aligned} \tag{13}$$

where F denotes resource biomass, Λ is the constant resource input rate, w is the (per capita) resource wash-out rate, and c is the resource (per capita) consumption rate by the prey. The prey birth rate b can be interpreted as $b = qc$, where q denotes the resource conversion efficiency. The equilibrium solution (assuming $m(C)$ to be independent of prey population size, but dependent on predator numbers, C) is:

$$F^* = \frac{m}{b}, \qquad N^* = \frac{1}{cm}(b\Lambda - mw), \tag{14a}$$

$$I^* = \frac{m}{\beta}(\mathrm{R}_0 - 1), \tag{14b}$$

$$p^* = \frac{cm^2}{\beta}\frac{(\mathrm{R}_0-1)}{(b\Lambda - mw)}, \tag{14c}$$

$$\mathrm{R}_0 = \frac{\beta N^*}{\gamma + m} = \frac{\beta(b\Lambda - mw)}{cm(\gamma+m)}. \tag{14d}$$

Assuming, as before, that the prey mortality rates are given by expression (3), the equilibrium resource level F^* linearly increases, whereas both the infective abundance I^* and the total prey abundance N^* decrease, with increasing predator abundance C. Fig. 6 plots p^*, I^* and N^* against C; prevalence again exhibits a unimodal hump-shaped pattern (Fig. 6A). As in the example of Fig. 3, the disease load I^* and prevalence p^* move in opposite directions in response to changes in low to moderate predation pressure (compare Figs. 6A and B), but now these patterns occur even with equal birth rates for all prey classes. The hump shape in p^* results because the prey

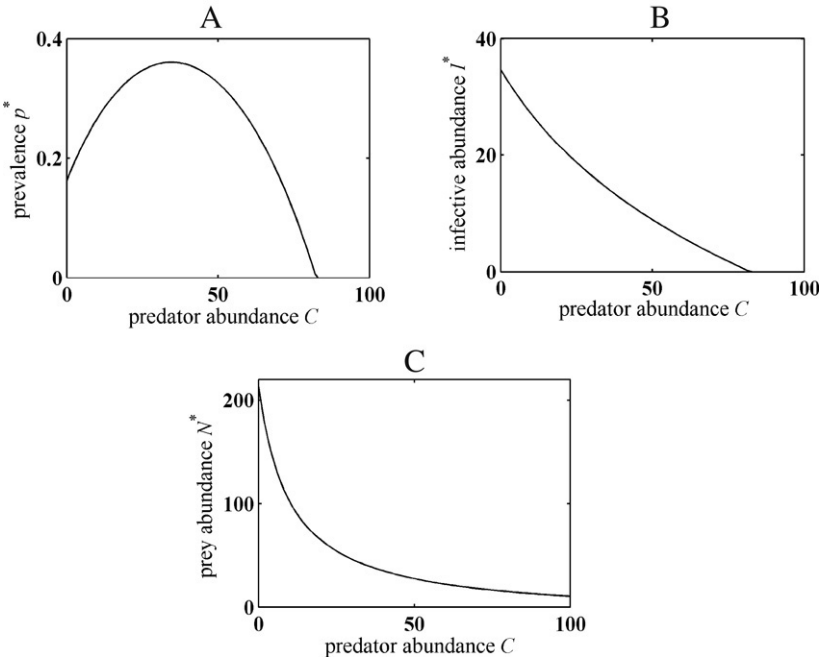

Fig. 6. Results are shown for equilibrium predator–prey–pathogen dynamics where prey consumes an explicit resource. A, Equilibrium prevalence p^* is plotted against predator abundance C (from (14c)). B, Equilibrium infective abundance I^* is plotted against C (from (14b)). C, Equilibrium prey abundance N^* is plotted against C (from (14a)). Model parameters are $b = 8$, $m_0 = 1$, $\beta = 1$, $\gamma = 5$, $a = 0.1$, $w = 1$ and $\Lambda = 2.8$.

abundance N^* decreases faster than I^* initially, which raises the prevalence before it finally begins to descend at higher levels of predation.

Again, permitting the predator to have a saturating numerical response can lead to unstable dynamics, even though predator numbers themselves are fixed (details not shown).

5. Discussion

Previous studies using simple host–pathogen models without acquired immunity have shown that predation on the host typically suppresses pathogen outbreaks in the host population, thereby indirectly benefiting the host and potentially the broader community by restricting "spillover" infection to novel hosts (Packer et al., 2003; Ostfeld and Holt, 2004; Hall et al., 2005). However, it has been recently recognized that counterintuitive patterns can arise when an immune host class is present, giving a hump-shaped pattern of prevalence against predation pressure (Holt and Roy, 2007). In this paper, we have demonstrated that this pattern is qualitatively robust to a wide range of realistic extensions of the basic SIR model, including different assumptions about host regulation, predator foraging, and the mechanism of disease transmission. Moreover, saturating predation can influence the stability of the host–pathogen dynamics, so that a stable equilibrium can change to unstable cycles via a Hopf type bifurcation, and the dynamics also exhibit alternative stable states. This complements the findings of Hall et al. (2005) for an SI model, and shows that unstable dynamics can occur even with acquired immunity in a broad range of models, even if predator numbers are fixed.

The hump-shaped pattern of pathogen prevalence against predation pressure arises from two distinct mechanisms (Holt and Roy, 2007). When the host is strongly regulated by density dependence, predation on recovered prey causes a compensatory increase in recruitment, and hence in the supply rate of fresh susceptibles that can "feed" the infection. Second, total host numbers and the abundance of infectives can respond in different degrees to changes in predation. In Fig. 1C, note that total host abundance declines linearly with increasing predation. But small amounts of predation increase the absolute abundance of infectives (Fig. 1B), due to density-dependent compensation in recruitment. Eventually, predation is sufficiently large to push down I^*, but more slowly than N^*, so prevalence still rises with predation (Fig. 1A). When the infectives are sufficiently depleted, of course, further increases in predation will then drive down prevalence.

In many of the examples we have presented, we assumed that the pathogen had no direct effect upon host mortality or fecundity. This greatly simplified the algebra and permitted analytic expression of equilibria. We should emphasize that the qualitative existence of a non-monotonic relationship between predation and prevalence, which we first showed elsewhere (Holt and Roy, 2007) and have explored in more detail in this paper, is not sensitive to this assumption. Relaxing it typically leads to much more complex algebra. However, for unstable dynamics to occur for predators with a fixed abundance but saturating functional responses, there must be some differences between prey classes in their demographic parameters and/or attack rates as a function of current or past infection (for example, in Figs. 2 and 3, we assume the fecundity of prey classes to be different). Without such differences, one can add all the compartments of the prey population in Eq. (1) to give the equation $dN/dt = bN(1 - dN) - [m_0 + aC/(1 + sN)]N$; this population can exhibit alternative stable states, but not

unstable dynamics. Thus, unstable dynamics in this model emerge from the interplay of parasitism, predation, and host heterogeneity.

Our results suggest that predation can eliminate pathogens via two distinct dynamical routes. First, at high predation the pathogen has an $R_0 < 1$, and so pathogen extinction is inevitable. Second, with a saturating response, high predation can lead to highly unstable dynamics, where epidemics are followed by a period of very low densities of infected individuals. In more realistic models incorporating stochasticity, it is likely that pathogens would risk extinctions during these phases of low abundance.

One way to get empirical traction with these results is to relate field estimates of prevalence to estimates of predator abundance. However, as we have noted above, prevalence p^* and the absolute abundance of infecteds I^* do not always respond to predation in the same way. Prevalence can be estimated from samples, whereas estimating the total density of infecteds in general will be much harder. Yet for some purposes, it is the latter quantity which one needs. For instance, to estimate the risk of spillover infection onto a novel host, it is more valuable to know I^* than p^*.

The take-home message from this study is that it may not be possible to generalize about how pathogen prevalence responds to predation on a host, unless one considers in detail the interplay of acquired immunity, host regulation and predator selectivity. Moreover, the combination of predation and infection can lead to unstable host dynamics and recurrent epidemics, when either factor alone entails stability. This can arise even with fixed predator numbers, and it is yet more likely when predator numbers respond dynamically to host density.

If there is no acquired immunity, the impact of predators will usually be to lower pathogen prevalence (Packer et al., 2003). Some taxa (e.g., many invertebrates) are believed to not have acquired immunity. For these species, the relationship of predation to disease levels may be simpler than that for taxa, like vertebrates, which have acquired immunity.

The disease models considered in this paper are fairly simple. Real host–pathogen systems have a variety of additional features, each of which could potentially influence the results presented here. Many host species exhibit age- and size-structured predation. For example, fish often show size-selective predation. Cats attack juvenile rats below certain sizes, but ignore bigger rats (Gregory E. Glass, pers. comm.). In addition, pathogen transmission itself can be age- or size-structured. In the residential areas of urban Baltimore, sub-adult rats in the size class of 100–200 g carry most of the pathogen load for several viral species, whereas transmission is apparently very low in adult rats weighing above 200 g (Childs et al., 1989). Such age- and size-structure effects in predation and disease transmission can have both ecological and epidemiological consequences for host–pathogen dynamics. Furthermore, host–pathogen dynamics often play out in spatially explicit settings. It is important to explore spatially explicit metapopulation models to examine the intertwined effects of predation and host–pathogen dynamics in distributed systems. All of these themes provide a challenge for future work.

Acknowledgments

We acknowledge the National Science Foundation (Grant# EF 0525751) and the University of Florida Foundation for support, G. E. Glass and two anonymous reviewers for their useful comments.

Appendix A. Local stability of equilibrium (4)

The Jacobian of Eq. (1) with $b_S = b_I = b_R \equiv b$ and $m_S = m_I = m_R \equiv m(C)$, evaluated at the equilibrium (4), is given by

$$\mathrm{J} = \begin{bmatrix} m(2-\mathrm{R}_0)-b & m-b-\gamma & 2m-b \\ m(\mathrm{R}_0-1) & 0 & 0 \\ 0 & \gamma & -m \end{bmatrix}.$$

The characteristic equation $\det(\mathrm{J}-\lambda\mathrm{I})=0$, where I is a 3×3 identity matrix, can be rearranged as $\lambda^3+a_1\lambda^2+a_2\lambda+a_3=0$, with the coefficients,

$$\begin{aligned} a_1 &\equiv m(\mathrm{R}_0-1)+b, \\ a_2 &\equiv m[b-m+(b+\gamma)(\mathrm{R}_0-1)], \\ a_3 &\equiv m(\gamma+m)(b-m)(\mathrm{R}_0-1), \\ a_1a_2-a_3 &= m(\mathrm{R}_0-1)[\gamma\mathrm{R}_0+b(\mathrm{R}_0-1)] \\ &\quad +b[b(\mathrm{R}_0-1)+(b-m)]. \end{aligned}$$

The Routh–Hurwitz criteria for local stability (p. 234, Edelstein-Keshet, 1988) require $a_1>0$, $a_3>0$ and $a_1a_2>a_3$, all of which hold with $\mathrm{R}_0>1$ (which implies $b>m$).

Appendix B. Estimating Lyapunov exponents from ODEs

The spectrum of Lyapunov exponents $\{\lambda_i\}$, $i=1,\ldots,n$, of a continuous dynamical system in an n-dimensional phase space is determined by monitoring the long-term stretching of an infinitesimal sphere of initial conditions as it evolves into an ellipsoid under the action of the dynamics. The ith Lyapunov exponent is defined in terms of the length of the ellipsoid's principal axis $p_i(t)$ (Wolf et al., 1985):

$$\lambda_i = \lim_{t\to\infty}\frac{1}{t}\ln\frac{p_i(t)}{p_i(0)}. \tag{B.1}$$

The center of the sphere traces a "fiducial" trajectory in the phase space, obtained by integrating the ODEs with an arbitrary initial condition. The n principal axes are given by an initially orthonormal vector frame anchored to the fiducial trajectory, and their evolution is determined by integrating the linearized equations (of the original ODEs) for n initial conditions. Because in a chaotic system each vector tends to align itself along the direction of the maximum growth, the Gram–Schmidt reorthonormalization (GSR) procedure is used repeatedly on the vector frame to retain its orthonormality (Wolf et al., 1985).

For our system we rewrite the three equations in (1) in terms of the variables N, I and R as follows

$$\begin{aligned}\frac{dN}{dt} &= [b_S(1-dN)-m_S]N \\ &\quad +[(b_I-b_S)(1-dN)-m_I+m_S]I \\ &\quad +[(b_R-b_S)(1-dN)-m_R+m_S]R, \\ \frac{dI}{dt} &= \beta NI-(\beta I+\gamma+m_I)I-\beta IR, \\ \frac{dR}{dt} &= \gamma I-m_R R.\end{aligned} \tag{B.2}$$

The fiducial trajectory given by (B.2) and the three ($n = 3$) infinitesimal principal axes are dynamically evolved by simultaneously integrating (B.2) along with nine other equations. These equations are given by linearizing (B.2) for the three principal axes, and can be compactly written as:

$$\begin{pmatrix} \frac{dn_1}{dt} & \frac{dn_2}{dt} & \frac{dn_3}{dt} \\ \frac{di_1}{dt} & \frac{di_2}{dt} & \frac{di_3}{dt} \\ \frac{dr_1}{dt} & \frac{dr_2}{dt} & \frac{dr_3}{dt} \end{pmatrix} = \begin{pmatrix} c_{11} & c_{12} & c_{13} \\ c_{21} & c_{22} & c_{23} \\ c_{31} & c_{32} & c_{33} \end{pmatrix} \begin{pmatrix} n_1 & n_2 & n_3 \\ i_1 & i_2 & i_3 \\ r_1 & r_2 & r_3 \end{pmatrix}, \tag{B.3}$$

where the orthonormal set (n_i, i_i, r_i), $i = 1, 2, 3$, denotes infinitesimal deviations from the fiducial trajectory $(N(t), I(t), R(t))$ for each of the three principal axes, and the matrix $\{c_{ij}\}$, $i, j = 1, 2, 3$, denotes the Jacobian of (B.2). Assuming a saturating mortality expression given by (7) and uniform predation ($a_S = a_I = a_R \equiv a$), we have

$$\begin{aligned} c_{11} &\equiv b_S[(1-dN)-d(N-I-R)] \\ &\quad -m_{S0}-\frac{aC}{(1+sN)^2}-d(b_I I+b_R R), \\ c_{12} &\equiv (b_I-b_S)(1-dN)-m_{I0}+m_{S0}, \\ c_{13} &\equiv (b_R-b_S)(1-dN)-m_{R0}+m_{S0}, \\ c_{21} &\equiv \left(\beta+\frac{aCs}{(1+sN)^2}\right)I, \\ c_{22} &\equiv \beta(N-2I-R)-\left(\gamma+m_{I0}+\frac{aC}{1+sN}\right), \\ c_{23} &\equiv -\beta I, \\ c_{31} &\equiv \frac{aCs}{(1+sN)^2}R, \qquad c_{32} \equiv \gamma, \\ c_{33} &\equiv -m_{R0}-\frac{aC}{1+sN}. \end{aligned}$$

The twelve equations in (B.2) and (B.3) are simultaneously integrated over a small time interval Δt with initial conditions $(N(0), I(0), R(0))$ and the 3×3 identity matrix respectively, where the identity matrix gives the initial orthonormal vector set. After the integration, the principal axes become stretched as well as slightly aligned along the direction of maximum growth due the action of the dynamics. The stretching factors of the three axes are computed as $p_i(t) = \sqrt{n_i(t)+i_i(t)+r_i(t)}$, and the vector set is again reorthonormalized following the GSR procedure (Wolf et al., 1985). This process is repeated after successive integration over Δt time intervals, and the Lyapunov spectrum is estimated using (B.1). As noted in the main text, using this procedure we found no evidence for chaotic dynamics in model 1 with a saturating functional response. This question is still open for the other models we have discussed.

Appendix C. Condition for mutual invasion and species coexistence in model (10)

Note that the model assumes the pathogen to be in effect a commensal of the host, so the coexistence problem is one-sided; the presence of the pathogen has no effect on the persistence of the predator. From (11b), the predator persists ($C^* > 0$) if

$$N^* < \frac{1}{d}\left(1-\frac{m_0}{b}\right). \tag{C.1}$$

Because we always assume $b > m_0$ (otherwise the prey becomes extinct), this condition implies $N^* < 1/d$. The pathogen persists ($I^* > 0$) if either $N^* > 1/d$ and $R_0 < 1$ (the predator becomes extinct under the first inequality), or $N^* < 1/d$ and $R_0 > 1$. The second set of conditions gives

$$N^* > \frac{b+\gamma}{bd+\beta}. \tag{C.2}$$

Combining (C.1) and (C.2), we get the condition (12) for a joint equilibrium of predator and pathogen ($C^*, I^* > 0$).

To find the condition under which the predator can invade the host–pathogen system in equilibrium, we rewrite the predator equation in (10):

$$\frac{1}{C}\frac{dC}{dt} = \varepsilon a\hat{N} - m_C,$$

where $\hat{N} = (1/d)(1 - m_0/b)$ is the equilibrium prey abundance in the absence of the predator. The invasion condition $(1/C)dC/dt > 0$ then gives $a\varepsilon(1 - m_0/b) > dm_C$, which is the same as (C.1) for predator persistence (using the expression for N^* from (11a)).

To obtain the condition for pathogen invasion in a predator–prey system in equilibrium, we likewise rewrite the equation for infective numbers from (10):

$$\frac{1}{I}\frac{dI}{dt} = \beta\tilde{S} - (\gamma + m_0 + a\tilde{C}),$$

where $\tilde{S} = \tilde{N} = m_C/a\varepsilon$ and $\tilde{C}$ (the same as N^* and C^* in (11a) and (11b)) give the equilibria in the absence of pathogen. With these expressions in the invasion condition, $(1/I)dI/dt > 0$ gives the inequality $a\varepsilon < m_C(\beta + bd)/(b + \gamma)$, which is the same as (C.2) for pathogen persistence.

Thus, inequality (12) gives the condition for pathogen and predator coexistence and also for mutual invasability.

More generally, one would expect the pathogen to impose demographic costs upon the host. In this case, the pathogen can potentially exclude the predator; alternative stable states (where one natural enemy excludes the other) are also possible. Anderson and May (1986) noted some historical examples where diseases in prey seemed to reduce predator numbers.

References

Abrams, P.A., 2002. Will small population sizes warn us of impending extinctions? Am. Nat. 160, 293–305.

Anderson, R.M., May, R.M., 1986. The invasion, persistence and spread of infectious diseases within animal and plant communities. Phil. Trans. R. Soc. Lond. B 314, 533–570.

Arneberg, P., Skorping, A., Grenfell, B., Read, A.F., 1998. Host densities as determinants of abundance in parasite communities. Proc. R. Soc. Lond. B 265, 1283–1289.

Borer, E.T., Briggs, C.J., Holt, R.D., 2007. Predators, parasitoids, and pathogens: A cross-cutting examination of intraguild predation theory. Ecology 88, 2681–2688.

Braza, P.A., 2005. Predator–prey dynamics with disease in the prey. Math. Biosci. Eng. 2, 703–717.

Chattopadhyay, J., Arino, O., 1999. A predator–prey model with disease in the prey. Nonlinear Anal. 36, 747–766.

Chattopadhyay, J., Pal, S., Abdllaoui, A.E., 2003. Classical predator–prey system with infection of prey population — a mathematical model. Math. Methods Appl. Sci. 26, 1211–1222.

Childs, J.E., Glass, G.E., Korch, G.W., LeDuc, J.W., 1989. Effects of hantaviral infection on survival, growth and fertility in wild rat (*Rattus norvegicus*) populations of Baltimore, Maryland. J. Wildlife Diseases 25, 469–476.

Collinge, S.K., Ray, C., 2006. Disease Ecology: Community Structure and Pathogen Dynamics. Oxford University Press, NY.

DeAngelis, D.L., Goldstein, R.L., O'Neill, R.V., 1975. A model for trophic interaction. Ecology 56, 881–892.

de Castro, F., Bolker, B.M., 2005. Parasite establishment and host extinction in model communities. Oikos 111, 501–513.

Dhooge, A., Govaerts, W., Kuznetsov, Y.A., 2003. MATCONT: A MATLAB package for numerical bifurcation analysis of ODEs. ACM TOMS 29, 141–164.

Dobson, A.P., 2004. Population dynamics of pathogens with multiple host species. Am. Nat. (Suppl.) 164, S64–S78.

Dwyer, G., Dushoff, J., Yee, S.H., 2004. The combined effects of pathogens and predators on insect outbreaks. Nature 430, 341–345.

Edelstein-Keshet, L., 1988. Mathematical Models in Biology. Random House, New York.

Hall, S.R., Duffy, M.A., Cáceres, C.E., 2005. Selective predation and productivity jointly drive complex behavior in host-parasite systems. Am. Nat. 165, 70–81.

Han, L., Ma, Z., Hethcote, H.W., 2001. Four predator–prey models with infectious diseases. Math. Comput. Modelling 34, 849–858.

Hethcote, H.W., Wang, W., Han, L., Ma, Z., 2004. A predator–prey model with infected prey. Theor. Popul. Biol. 66, 259–268.

Hochberg, M.E., Hassell, M.P., May, R.M., 1990. The dynamics of host-parasitoid-pathogen interactions. Am. Nat. 135, 74–94.

Holt, R.D., Dobson, A.P., 2006. Extending the principles of community ecology to address the epidemiology of host-pathogen systems. In: Collinge, S.K., Ray, C. (Eds.), Disease Ecology: Community Structure and Pathogen Dynamics. Oxford University Press, NY, pp. 6–27.

Holt, R.D., Polis, G.A., 1997. A theoretical framework for intraguild predation. Am. Nat. 149, 745–764.

Holt, R.D., Roy, M., 2007. Predation can increase the prevalence of infectious disease. Am. Nat. 169, 690–699.

Hudson, P.J., Dobson, A.P., Newborn, D., 1992. Do parasites make prey vulnerable to predation? Red grouse and parasites. J. Animal Ecology 61, 681–692.

Keesing, F., Holt, R.D., Ostfeld, R.S., 2006. Effects of species diversity on disease risk. Ecol. Lett. 9, 485–498.

Murdoch, W.W., Briggs, C.J., Nisbet, R.M., 2003. Consumer-Resource Dynamics. Princeton University Press, Princeton, NJ.

Ostfeld, R.S., Holt, R.D., 2004. Are predators good for your health? Evaluating evidence for top-down regulation of zoonotic disease reservoirs. Frontiers Ecol. Environ. 2, 13–20.

Packer, C., Holt, R.D., Dobson, A.P., Hudson, P., 2003. Keeping the herds healthy and alert: Impacts of predation upon prey with specialist pathogens. Ecol. Lett. 6, 797–802.

Rohani, P., Wearing, H.J., Vasco, D.A., Huang, Y., Understanding host-multi-pathogen systems: the interaction between ecology and immunology. In: Ostfeld, R.S., Keesing, F., Eviner, V. (Eds.), Ecology of Infectious Diseases, Princeton University Press, NJ (in press).

Rosenzweig, M.L., 1971. The paradox of enrichment: Destabilization of exploitation ecosystems in ecological time. Science 171, 385–387.

Turchin, P., 2003. Complex Population Dynamics. Princeton University Press, Princeton, NJ.

Wolf, A., Swift, J.B., Swinney, H.L., Vastano, J.A., 1985. Determining lyapunov exponents from a time series. Physica D 16, 285–317.

Woolhouse, M.E.J., Taylor, L.H., Haydon, D.T., 2001. Population biology of multihost pathogens. Science 292, 1109–1112.

Xiao, Y., Chen, L., 2001. Modeling and analysis of a predator–prey model with disease in the prey. Math. Biosci. 171, 59–82.